Part IV

Silicon isotopic variations in soils

Chapter 10

Silicon isotopic fractionation during adsorption of aqueous monosilicic acid onto iron oxide *

Abstract

The quantification of silicon isotopic fractionation by biotic and abiotic processes contributes to the understanding of the Si continental cycle. In soils, light Si isotopes are selectively taken up by plants, and concentrate in secondary clay-sized minerals. Si can readily be retrieved from soil solution through the specific adsorption of monosilicic acid ($H_4SiO_4^0$) by iron oxides. Here we report on the Si isotopic fractionation during $H_4SiO_4^0$ adsorption on synthesized ferrihydrite and goethite in batch experiment series designed as function of time (0-504h) and initial concentration (ic) of Si in solution (0.21-1.80 mM), at 20°C, constant pH (5.5) and ionic force (1 mM). At various contact times, the δ^{29}Si vs. NBS28 compositions were determined in selected solutions (ic = 0.64 and 1.06 mM Si) by MC-ICP-MS in dry plasma mode with external Mg doping with an average precision of ± 0.08‰ (± $2\sigma_{SEM}$). Per oxide mass, ferrihydrite (74-86% of initial Si loading) adsorbed more

*Adapted from Delstanche S., Opfergelt S., Cardinal D., Elsass F., André L., Delvaux B. Silicon isotopic fractionation during adsorption of aqueous monosilicic acid onto iron oxide. Submitted to *Geochimica Et Cosmochimica Acta*.

Si than goethite (37-69%) after 504h of contact over the range of initial Si concentration 0.42-1.80 mM. Measured against its initial composition (δ^{29}Si = +0.01 ± 0.04‰ (± $2\sigma_{SD}$)), the solution was systematically enriched in ^{29}Si, reaching maximum δ^{29}Si values of +0.70 ± 0.07‰ for ferrihydrite and +0.50 ± 0.08‰ for goethite for ic 1.06mM. The progressive ^{29}Si enrichment of the solution fitted a Rayleigh distillation path. The fractionation factor $^{29}\varepsilon$ (± $1\sigma_{SD}$) was -0.56 ± 0.01‰ for ferrihydrite and -0.83 ± 0.03‰ for goethite. Our data imply that the sorption of $H_4SiO_4^0$ onto synthetic iron oxides produced a Si isotopic fractionation similar or larger to that generated by Si uptake by plants and diatoms. They further suggest that the concentration of light Si isotopes in the colloidal fraction of soils is partly due to $H_4SiO_4^0$ sorption onto secondary clay-sized iron oxides.

10.1 Introduction

Mineral weathering releases elements from the lithosphere, allowing them to participate in biogeochemical processes in terrestrial and aquatic ecosystems. Silicon is the second mass abundant element of the Earth's crust and a major solute in river discharge into oceans (Gaillardet et al., 1999; Tréguer et al., 1995). Breakdown of primary silicates, translocation of Si in solution, formation of secondary silicates, and Si uptake by plants are involved in the continental cycle of Si. Dissolved Si is present as monosilicic acid ($H_4SiO_4^0$) in natural solutions (Lindsay, 1979), where it is commonly a major solute (McKeague and Cline, 1963c). Apart from clay formation and uptake by biota, monosilicic acid can be withdrawn from soil solution through its sorption onto aluminium and iron oxides (Beckwith and Reeve, 1963; Jones and Handreck, 1963; McKeague and Cline, 1963c). Iron oxides are ubiquitous in sediments, weathered rocks and soils (Schwertmann and Taylor, 1989), where they readily control the concentration of aqueous silicic acid (Gehlen and Van Raaphorst, 2002; McKeague and Cline, 1963c). Their surface OH groups specifically interact with silicic acid by exchanging ligands to form a bi-dendate innersphere complex involving monomeric $SiO_2(OH)_2^{2-}$ as main adsorbed species at low loading of aqueous Si (below ∼0.9 mM) (Davis et al., 2002; Hansen et al., 1994b; Hiemstra et al., 2007; Hingston et al., 1967; Pokrovski et al., 2003; Sigg and Stumm, 1981; Swedlund and Webster, 1999). At higher loading of aqueous Si, however, Si tetramer can form on goethite surface (Hiemstra et al., 2007), whereas $H_4SiO_4^0$ polymerization occurs on ferrihydrite surface at $H_4SiO_4^0$ concentrations below those required

for polymerization in solution (Swedlund and Webster, 1999). The adsorption of Si by Fe oxides strongly varies with pH, and commonly reaches a maximum around pH 9 (Hansen et al., 1994a; Hiemstra et al., 2007; Jones and Handreck, 1963; Sigg and Stumm, 1981; Swedlund and Webster, 1999).

Following weathering, iron oxides accumulate in soils (Bikerland, 1974), where they appear as both crystalline and short-range ordered (sro) minerals mainly in their clay-sized fraction (Schwertmann and Taylor, 1989). They can exert a crucial impact on the retention of Si and the control of aqueous $H_4SiO_4^0$ (McKeague and Cline, 1963c). Quantifying the fractionation of Si stable isotopes by biotic and abiotic processes readily contributes to the understanding of the continental cycle of Si. As inferred from δ^{29}Si and/or δ^{30}Si values, river waters are depleted in light Si isotopes (Alleman et al., 2005; De La Rocha et al., 2000; Ding et al., 2004; Georg et al., 2006a 2007c) compared to crustal rocks (Douthitt, 1982), following fractionating processes of silicate weathering and formation of clay-sized minerals (Ziegler et al. (2005ab), Chapter 8), silcrete formation (Basile-Doelsch et al., 2005), and Si uptake by biota (De La Rocha et al., 1997; Ding et al., 2005b 2008; Opfergelt et al., 2006ab) (Chapter 7; Appendix C).

In this paper, we report on an experimental study on the isotope fractionation of Si by $H_4SiO_4^0$ adsorption onto iron oxide. The experiments were designed to answer four questions of critical environmental significance: (1) Does Si isotope fractionation occur during Si adsorption onto Fe oxide at common pH for soil solutions? (2) How much does this fractionation compare with that generated by Si uptake by biota? Can this fractionation contribute to (3) the depletion of light Si isotopes in river waters, and (4) the enrichment of light Si isotopes in clay-sized soil fractions? For these purposes, we use goethite and ferrihydrite, respectively crystalline and sro minerals. Our experimental study involves the prior synthesis and characterization of pure Fe oxides and the quantitative determination of $H_4SiO_4^0$ adsorption in controlled conditions of temperature, solid:liquid ratio, pH and ionic force.

10.2 Materials and methods

At all steps, acid-washed high density polyethylene (HDPE) ware and analytical grade *Pro Analysi* chemicals were used to minimise Si contamination.

10.2.1 Synthesis and characterization of ferrihydrite and goethite

Ferrihydrite and goethite were synthesized according to the methods described in Cornell and Schwertmann (1996). For ferrihydrite, a freshly prepared 0.1M $Fe(NO_3)_3$ solution (250 ml) was slowly neutralized by 1M NaOH (70 ml), i.e. brought drop wise to pH 7.5. The red/brown precipitate was separated by centrifugation (3500 rpm, 10 min), dialysed (dialysis-membrane SPECTRA/POR 4, MWCO = 12-14000, ∅=29mm) against deionized water until electrical conductivity was stable at 1-2 μS for 4h. The dialyzed product was freeze-dried. For goethite, a freshly prepared 1M $Fe(NO_3)_3$ (100 ml) solution was neutralized by 5M NaOH (70 ml) under intense stirring and brought to pH >12. The red/brown precipitate was dried in the mother liquid at 70°C for 60h, and turned to yellow/brown. The precipitate was washed with deionized water through washing-centrifugation cycles (13100 rpm, 15 min) until pH and electrical conductivity were stable respectively at 5.5 and 1-2 μS. The precipitate was oven-dried at 50°C for 48h. Mineralogical and chemical characterizations of both products were done by X-ray diffraction (XRD, Bruker D8 Advance diffractometer), transmission electron microscopy (TEM, Philips 420 STEM), elemental analysis (inductively coupled plasma-atomic emission spectrometry: ICP-AES, Jarrell Ash Iris Advantage), after Na_2O_2 fusion in vitrified graphite crucibles at 1000°C, dithionite-citrate-bicarbonate extraction (DCB, Mehra and Jackson (1960)), dark oxalate extraction (Blakemore et al., 1981) and surface area determination using ethylene glycol monoethyl ether (EGME, Carter et al. (1965)).

Table 10.1: Chemical analysis of synthesized ferrihydrite and goethite: Average contents of DCB (d) and oxalate (o) extractable Fe (Fe_d, Fe_o; n=2), and of total Si (Si_t; n=5), and KH_2PO_4 extractable Si content ($Si_{KH_2PO_4}$).

	Fe_d $g.kg^{-1}$	Fe_o $g.kg^{-1}$	Fe_o:Fe_d	Si_t $g.kg^{-1}$	$Si_{KH_2PO_4}$ $mg.kg^{-1}$
Ferrihydrite	594	513	0.864	0.12	5.7
Goethite	607	2.5	0.004	0.16	5.9

The X-ray diffraction (XRD) patterns were consistent with those for 2-line ferrihydrite and goethite in Cornell and Schwertmann (1996), and in Jambor and Dutrizac (1998) (Figure 10.1). Observations by TEM revealed the common micro-aggregated shape of ferrihydrite, and the typical euhedral acicular crystals (0.5-1.5 mm length) of goethite, constituted of parallel subunits (Figure 10.2) (Cornell and

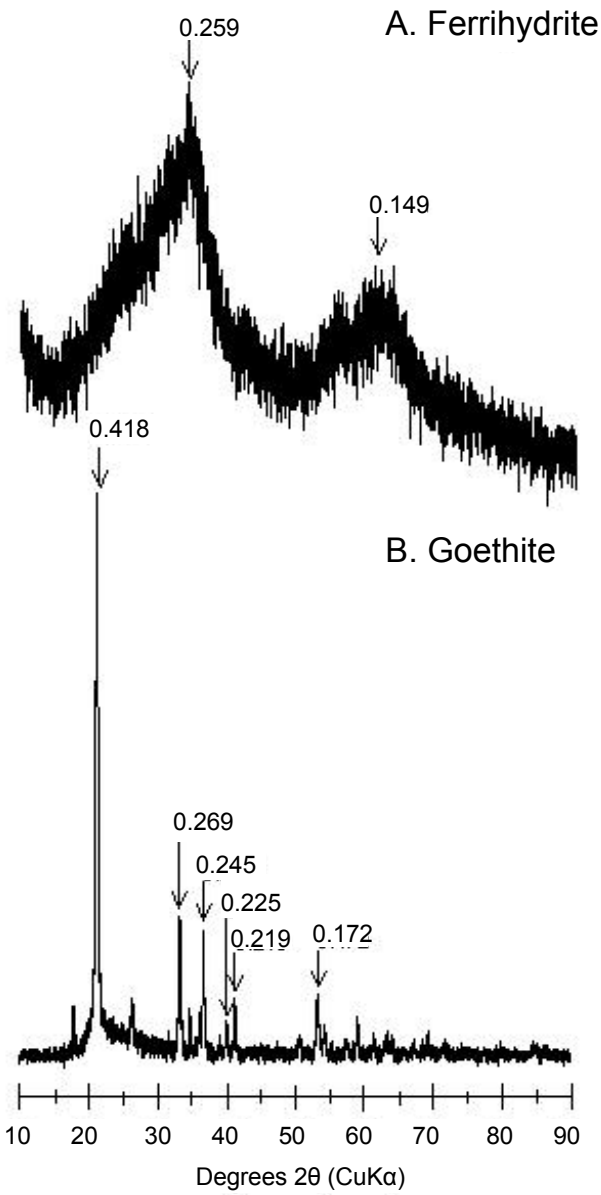

Figure 10.1: Cu Kα X-ray diffraction patterns of the synthesized (A) 2-line ferrihydrite and (B) goethite. Major peaks are labeled in nm.

Schwertmann, 1996; Schwertmann and Taylor, 1989). The content of poorly crystalline Fe was assessed through the determination of the ratio of oxalate extractable Fe (Fe_o) to DCB extractable Fe (Fe_d) (Cornell

and Schwertmann, 1996) (Table 10.1). The Fe_o:Fe_d ratio was 0.004 for goethite, certifying a well crystalline form, and 0.864 for ferrihydrite, attesting a large dominance of sro mineral particles. The average concentration of Si in the synthesized ferrihydrite and goethite was below 0.2 g kg^{-1} (Table 10.1), revealing the very low level of Si contamination. A specific extraction of adsorbed Si by KH_2PO_4 (Delfosse et al., 2005a) showed that adsorbed Si was negligible and represents less than 0.5% of the total Si budget per experiment (Table 10.1). The EGME specific surface was 338 and 147 m^2 g^{-1} for ferrihydrite and goethite, respectively.

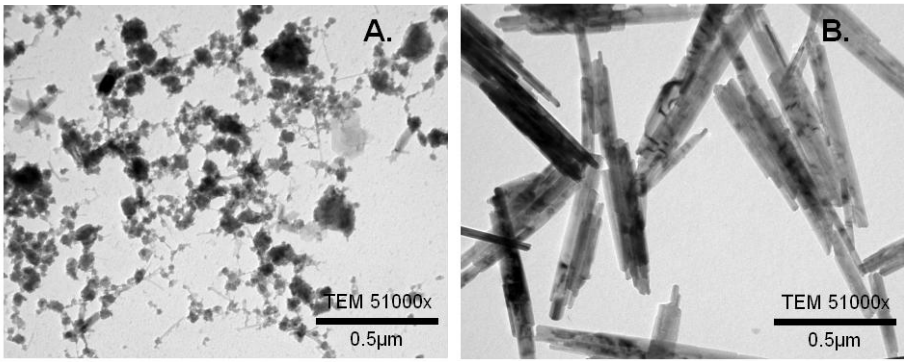

Figure 10.2: TEM micrographs of the synthesized (A) 2-line ferrihydrite and (B) goethite (with a 51000-magnification for both images), from aliquots of $<2\mu$m-suspensions left air-dried on a C-coated Cu-grid.

10.2.2 Adsorption experiments

$H_4SiO_4^0$ solutions were prepared by dissolving $Na_2SiO_3.5H_2O$ in MilliQ water, and further leaching on an H^+ cation exchanger (Amberlite® IR-120) to fix Na^+ ions. The leaching was terminated when the threshold level of sodium was below 10^{-2} mM Na, as determined by ICP-AES (Henriet et al., 2006). The acidic Si stock solution (35.61 mM Si) was free of polymers (Beckwith and Reeve, 1963; Stumm and Morgan, 1996). Eight solutions of distinct initial concentrations (ic) of Si were considered: 0.21, 0.42, 0.64, 0.85, 1.06, 1.29, 1.49 and 1.80 mM Si. The ic solutions were prepared by using MilliQ water and pure $NaNO_3$. A background electrolyte concentration of 1 mM $NaNO_3$ was used throughout to maintain ionic force constant. Contact between ic Si solution and Fe oxide was made in HDPE bottles, on a reciprocating

shaker in a dark room at 20°C. A suspension of 5 g of Fe oxide was transferred to a dialysis-membrane (SPECTRA/POR 4; MWCO 12-14000; ∅=16mm) and plunged in the Si solution of given ic. The initial solution volume was 1000 ml, as gravimetrically determined (1 g:250 ml solid:liquid ratio). The pH was adjusted to the target pH 5.5±0.2 by addition of 1 M NaOH or 0.7 M HNO_3. The target pH value is common for natural waters in equilibrium with atmospheric CO_2. During the experiment, pH was regularly checked and adjusted to the target when necessary, and systematically checked one hour before sampling solutions.

The adsorption experiments were done in triplicates: series 1 and 2 were used to provide adsorption data whereas series 3 was used for the determination of Si isotopes. For series 1 and 2, solution aliquots (10 ml) were sampled, respectively after 6, 12, 24, 48, 72, 96, 192, 288, 408 and 504 h of contact time between Fe oxide and Si solution, and kept in HDPE bottles. The aliquots from each solution were transferred to polyethylene scintillation vials, then acidified by adding 50 μl of 7M HNO_3 and stored in the dark at 4°C prior to further analysis. The Si sorption experiments were conducted in triplicate. Series 1 and 2 provided solution aliquots to determine the bulk concentrations of Si, as determined by ICP-AES (Jarrell Ash Iris Advantage, detection limit $<$ 0.7 μM Si). Adsorbed Si was computed as the difference between the Si solution concentrations before and after contact with Fe oxide.

10.2.3 Isotopic composition of solutions at given contact times

Two ic solutions (0.64 and 1.06 mM Si) and twenty solution aliquots from series 3 were selected on the basis of adsorption data with respect to detection limit required for Si isotope measurement. Dissolved Si in the chosen samples was purified by triethylamine molybdate co-precipitation and combustion in covered Pt crucibles at 1000°C (De La Rocha et al., 1996), and dissolved in dilute suprapur HF-HCl mixture (Cardinal et al., 2003). Si isotopes were measured using a Nu Plasma MC-ICP-MS operating in dry plasma mode, with an external Mg doping to correct mass bias (Cardinal et al., 2003). The analytical method was supported by an inter-laboratory comparison exercise and proved to be accurate on secondary reference materials (Reynolds et al. (2007); Chapter 6). The average precision on δ^{29}Si was ± 0.08‰ ($\pm 2\sigma_{SEM}$). The results are presented as δ^{29}Si (‰), expressing the ^{29}Si/^{28}Si ratios of our samples relative to those of the NBS28 silica sand standard (National Institute of Standard and Technology RM #8546) for silicon isotopes (Carignan

et al., 2004):

$$\delta^{29}\mathrm{S}i = \left[\frac{\left(\frac{^{29}\mathrm{S}i}{^{28}\mathrm{S}i}\right)_{\text{sample}}}{\left(\frac{^{29}\mathrm{S}i}{^{28}\mathrm{S}i}\right)_{\text{NBS28}}} - 1 \right] \times 1000 \qquad (10.1)$$

Very small concentrations (below 0.5% of the total Si budget per experiment) of initial adsorbed Si should not affect the isotopic composition of our solutions. Indeed, a contamination of ± 0.08‰ equivalent to our $2\sigma_{SEM}$ should be induced by initial adsorbed Si displaying an isotopic composition of - 48‰ or +49‰, which is very unlikely regarding Si isotopic variations on Earth (Basile-Doelsch, 2006).

10.3 Results and discussion

Mineralogical and chemical characterizations show that the separate synthesized products were genuine ferrihydrite and goethite minerals.

10.3.1 Monomeric silicon adsorption by ferrihydrite and goethite

Only the average values of the duplicates are presented in following text, tables and figures. The error bars are systematically presented in the figures, and show the experimental reproducibility. Table 10.2 presents the average bulk concentrations of Si in each solution corresponding to ferrihydrite and goethite, and to the respective eight ic solutions and ten contact times. The amount of KH_2PO_4-desorbed Si from synthesized Fe oxide (Table 10.1) are extremely low (<5%) as compared to adsorbed Si (Table 10.2), confirming the negligible Si contamination during oxide synthesis. For both Fe oxides and each ic solution, the concentration of aqueous Si readily decreases with increasing contact time, revealing net Si adsorption. Below pH 9, the solution speciation of $H_4SiO_4^0$ is pH independent, meaning that only aqueous $H_4SiO_4^0$ was present in significant concentrations (Hiemstra et al., 2007). The systematic adjustment at pH 5.5±0.2 required a surplus addition of NaOH for ferrihydrite, indicating a net proton release during adsorption; the surplus addition of NaOH was very low for goethite. In our controlled pH conditions, the H^+ release is likely caused by the specific interaction of $H_4SiO_4^0$ with OH groups of oxide surface involving ligand exchange under formation of a Fe oxide-monosilicate surface complex ($\equiv Fe_2O_2Si(OH)_2$ bi-dendate complex) (Hansen et al., 1994a; Hiemstra et al., 2007; Sigg and Stumm, 1981). At Si concentration above ~0.2 mM, a surface Si tetramer ($\equiv Fe_2O_2SiOHOSi_3O_3(OH)_9$) may have formed on goethite

surface; at pH 5.5, the proportion of this surface tetramer would be below ∼25%, and the monomer species should be largely dominant (Hiemstra et al., 2007). The maximum value of the mole ratio of aqueous Si to ferrihydrite-Fe was 0.03. In these conditions, the only significant surface bonding of $H_4SiO_4^0$ with ferrihydrite surface should be the surface complexation of monomeric $H_4SiO_4^0$ (Swedlund and Webster, 1999). This interpretation is consistent with the adsorption data performed at pH 3-6 by Hansen et al. (1994a).

Table 10.2: Average values of Si concentration (mM Si) in solution as a function of contact time and type of Fe oxide for each initial Si concentration (time 0).

Time (h)	0	6	12	24	48	72	96	192	288	408	504
Ferrihydrite	0.21	0.20	0.19	0.19	0.17	0.16	0.15	0.13	0.12	0.09	0.08
	0.42	0.39	0.38	0.35	0.31	0.27	0.24	0.15	0.14	0.10	0.08
	0.64	0.61	0.57	0.51	0.45	0.40	0.36	0.25	0.17	0.12	0.09
	0.85	0.79	0.75	0.69	0.60	0.53	0.47	0.31	0.23	0.17	0.13
	1.06	1.01	0.96	0.90	0.82	0.74	0.69	0.43	0.41	0.33	0.27
	1.29	1.21	1.16	1.07	0.97	0.88	0.81	0.61	0.47	0.38	0.32
	1.49	1.39	1.33	1.25	1.12	1.02	0.95	0.75	0.60	0.49	0.43
	1.80	1.68	1.62	1.55	1.43	1.33	1.23	0.99	0.81	0.65	0.56
Goethite	0.21	0.19	0.19	0.17	0.15	0.13	0.12	0.10	0.08	0.07	0.06
	0.42	0.39	0.37	0.33	0.29	0.25	0.22	0.16	0.15	0.14	0.13
	0.64	0.58	0.55	0.50	0.44	0.38	0.35	0.29	0.29	0.28	0.27
	0.85	0.80	0.78	0.72	0.65	0.60	0.57	0.49	0.47	0.45	0.43
	1.06	0.99	0.95	0.87	0.77	0.74	0.71	0.66	0.63	0.60	0.57
	1.29	1.18	1.14	1.08	1.00	0.95	0.90	0.83	0.79	0.77	0.73
	1.49	1.42	1.37	1.31	1.23	1.15	1.14	1.03	0.98	0.95	0.90
	1.80	1.71	1.65	1.58	1.49	1.43	1.37	1.28	1.23	1.08	1.13

10.3.2 Quantitative silicon adsorption by ferrihydrite and goethite

In fixed conditions of pH, ionic force, temperature and solid:liquid ratio, the Si amount adsorbed depends on reaction time and type of Fe oxide (Hansen et al., 1994a). Per oxide mass, ferrihydrite generally adsorbs more Si than goethite (Table 10.2). After 504h of contact between Fe oxide and Si solution, the fraction of adsorbed Si ranges between 63 and 86% for ferrihydrite, and between 37 and 72% for goethite (Figure 10.3). Few studies have shown a larger Si adsorption by ferrihydrite over goethite (Hansen et al., 1994a), or by amorphous over crystalline Fe oxide (Jones and Handreck, 1963). Surface reactivity for oxyanions, weak acids and water is well known to decrease with

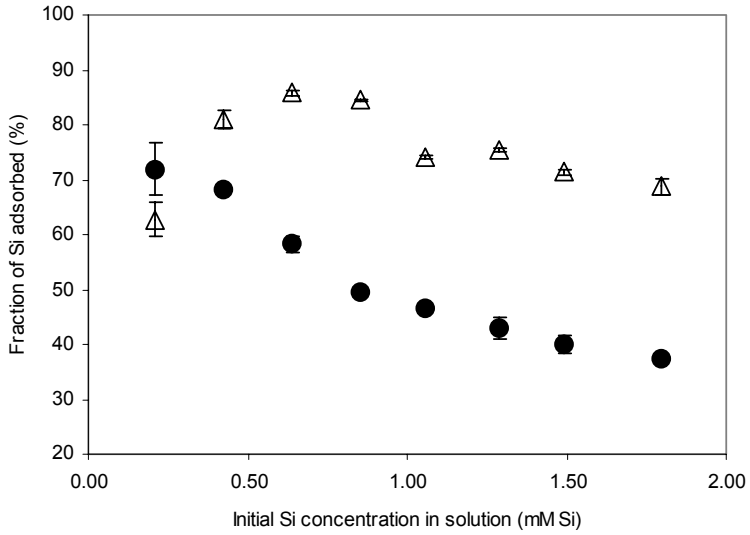

Figure 10.3: Average values (n=2) of adsorbed Si, expressed as a fraction of initial Si after 504 hours of contact. Ferrihydrite: open triangle. Goethite: full circle.

increasing Fe oxide crystallinity (Cornell and Schwertmann, 1996; Parfitt, 1978; Schwertmann et al., 1985; Schwertmann and Taylor, 1989). As crystallinity increases, oxide crystals become larger and surface area decreases (Schwertmann et al., 1985). As measured by EGME retention, the surface area was 338 m^2 g^{-1} for ferrihydrite and 147 m^2 g^{-1} for goethite (see section 10.2.1). As expected (Cornell and Schwertmann, 1996), these EGME values are generally above BET-N_2 values previously measured for synthesized Fe oxides: 35-87 m^2 g^{-1} for goethite (Garman et al., 2004; Hansen et al., 1994a; Luxton et al., 2006; Waltham and Eick, 2002), 269-380 m^2 g^{-1} for ferrihydrite (Hansen et al., 1994ab; Hofmann et al., 2004). In agreement with Cornell and Schwertmann (1996), we believe, however, that there is large uncertainty about the surface area measurement of hydrous hydroxyl-bearing Fe oxide because this measurement requires a prior anhydrous vacuum. This conditioning can, indeed, modify surface particle, particle size and porosity through particle microaggregation (Hofmann et al., 2004).

The adsorption data are illustrated at 504h contact time in Figure 10.4. Under the hypothesis that equilibrium was reached after 504h contact time, the data could be fitted to Freundlich, Langmuir, Temkin and Redlich-Peterson adsorption isotherms (not shown). For goethite,

the adsorption data (Q, C) best fit a Freundlich isotherm expressed as:

$$\mathrm{Q} = K_F \mathrm{C}^{1/n} \tag{10.2}$$

where Q is the Si adsorbed per unit mass of oxide (mmol Si g^{-1}), K_F and n are empirical constants and C the $H_4SiO_4^0$ concentration of the solution (mM Si). This empirical model has been considered to be thermodynamically consistent with sorption on heterogeneous surfaces that imply different sorption sites and affinities (Weber et al., 1991). However, this is also consistent with the fact that the positive charge of Fe oxide surface decreases with the increase in the surface Si loading (Anderson and Benjamin, 1985; Hiemstra et al., 2007; Hingston et al., 1972), since the net proton release leads to a shift in the isoelectric point of Fe oxide (Garman et al., 2004; Luxton et al., 2006). For ferrihydrite, the adsorption data best fit a Temkin isotherm expressed as:

$$\ln\mathrm{Q} = A + B \ln\mathrm{C} \tag{10.3}$$

where Q and C are defined as in Eq.(10.2), and A and B are constants determined through linear regression from experimental data. The Temkin equation implies the condition that the energy of adsorption decreases linearly with surface coverage (Parfitt, 1978). This is consistent with the decrease of charge density as proposed for goethite. As discussed here above, the much larger adsorption of Si on ferrihydrite in the range 0.1-0.6 mM Si is attributed to the larger availability of reactive sites in ferrihydrite relative to goethite.

10.3.3 Adsorption kinetics

Si adsorption increases with time, first rapidly, then more slowly (Table 10.2). The time dependent adsorption of Si by Fe oxide is illustrated for the ic solutions 0.64 and 1.06 mM Si (Figure 10.5). Si adsorption requires days-weeks. The rate of adsorption is rather large during the first hours (∼50h for goethite, ∼100h for ferrihydrite), then decreases. After ∼200h for goethite and ∼300h for ferrihydrite, it seems to reach a constant value, which increases from goethite to ferrihydrite with increasing aqueous Si concentration. These observations are in very good agreement with previous results (Hansen et al., 1994ab). Kinetic data are well fitted to pseudo-second order and parabolic diffusion models, but poorly to the Elovich equation (not shown). The change in the rate of Si adsorption onto ferrihydrite is similar to that observed for phosphate (Bolan et al., 1985; Lijklema, 1980). The slow adsorption step for phosphate has been attributed to diffusion into interparticle

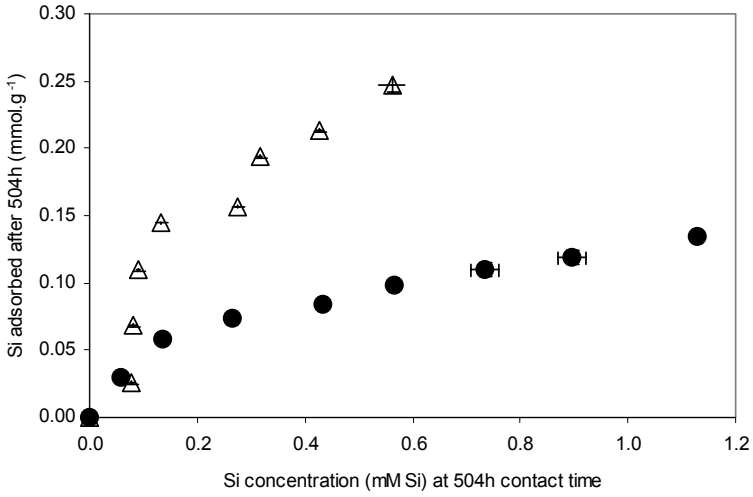

Figure 10.4: Average values of Si adsorbed (n=2) as a function of Si concentration of the solution after 504h contact time. Ferrihydrite: open triangle. Goethite: full circle.

pores (Willett et al., 1988), whereas arsenate adsorption onto ferrihydrite has been successfully predicted using a pore-space diffusion model and assuming rapid adsorption at external surfaces of aggregates (Fuller et al., 1993). Accordingly, and in agreement with Hansen et al. (1994b), the rate of Si adsorption observed here is probably controlled by rapid interaction of monosilic acid with external oxide surface sites, and by interparticle diffusion.

10.3.4 Silicon isotopic fractionation during adsorption of monosilic acid

The selected solutions correspond to the ic solutions 0.64 mM Si and 1.06 mM Si at various contact times ranging, respectively, between 0 and 192h, and 0 to 504h. The values of Si concentration in the selected solutions at pH 5.5 range between 0.25 and 0.96 mM Si (Table 10.2). These conditions of pH and Si concentration imply a dominant adsorption of monomeric Si (Hansen et al., 1994ab; Hiemstra et al., 2007; Sigg and Stumm, 1981; Swedlund and Webster, 1999), but do not exclude the occurrence of a surface Si tetramer on goethite surface. For Si solutions oversaturated with respect to quartz ($K_S > \sim 0.12$ mM Si), the proportion of surface Si tetramer was estimated below 15% for Si concentration below $\sim$ 1 mM Si (Hiemstra et al., 2007). The Si isotopic

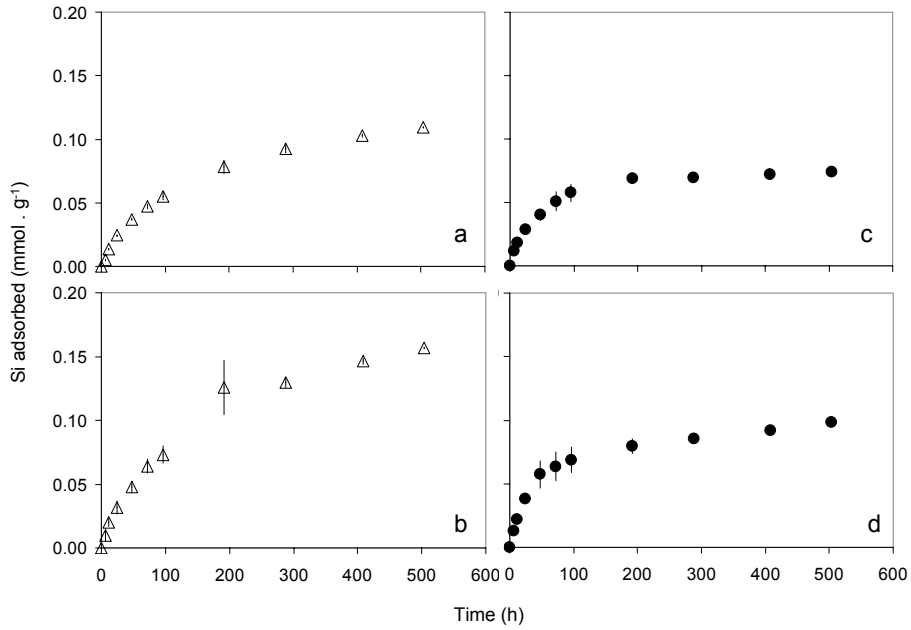

Figure 10.5: Average values of the concentration of Si adsorbed (n=2) by ferrihydrite (a: 0.64mM Si ic - b: 1.06mM Si ic) and goethite (c: 0.64mM Si ic - d: 1.06mM Si ic), as a function of contact time.

compositions of the selected solutions are given in Table 10.3. The δ^{29}Si value significantly increases with increasing time, and thus with decreasing Si concentration of the solution at various contact times. This increase involves a gradual fractionation of stable Si isotopes, revealing a depletion of the aqueous phase in light Si isotopes which parallels the adsorption of monosilicic acid onto Fe oxide. Measured against its initial composition ($+0.01 \pm 0.04$‰ ($\pm 2\sigma_{SD}$)), the solution is indeed systematically enriched with the heavy isotope, reaching a maximum δ^{29}Si-value of $+0.70 \pm 0.07$‰ for ferrihydrite and $+0.50 \pm 0.08$‰ for goethite at ic 1.06 mM Si after 504 h of contact. For ferrihydrite at ic 0.64mM Si, the isotopic compositions measured in solution after 72h and 192h are shifted down compared to the global trend (Table 10.3). This shift could be attributed to an abnormal variation of pH during the experiment at 72h in this series (series 3 used only for isotopic measurements, see section 10.2.3). The pH variation may have likely influenced the isotopic composition of the solutions at contact time $\geqslant$ 72h, because pH affects the adsorption of Si onto Fe oxide (Jones and

Handreck, 1963). These two measurements at 72 and 192h will thus not be considered in further calculations and interpretation. The isotopic composition of the solution can be predicted by following models: the Rayleigh model following:

$$\delta^{29}Si_{\text{solution}} = \delta^{29}Si_{\text{initial}} + {}^{29}\varepsilon_R \ln f \tag{10.4}$$

the steady state model following:

$$\delta^{29}Si_{\text{solution}} = \delta^{29}Si_{\text{initial}} - {}^{29}\varepsilon_S (1 - f) \tag{10.5}$$

where $\delta^{29}Si_{\text{initial}}$ and $\delta^{29}Si_{\text{solution}}$ are respectively measured in the ic solution and the solution at each contact time (Table 10.3), f is the fraction of Si remaining in solution at each contact time (Table 10.2), and ${}^{29}\varepsilon$ is the fractionation factor (R for Rayleigh, S for steady state).

From Eq.(10.4) and (10.5), a fractionation factor ${}^{29}\varepsilon$ for the adsorption process can be computed following both models (Table 10.4). The uncertainty on ${}^{29}\varepsilon$ is the error on the slope ($1\sigma_{SD}$) of $\delta^{29}Si_{\text{solution}}$ data plotted against ln f or (1 - f) for Rayleigh and steady state model, respectively. It was calculated using the REG procedure of the SAS System (version 9.1 for Windows, SAS Institute, Cary, NC, USA). The ${}^{29}\varepsilon$ values are presented in Table 10.4.

Table 10.3: Measured Si isotopic compositions (δ^{29}Si vs.NBS28) of the solution, as a function of initial Si concentration (0.64 mM and 1.06 mM Si), contact time (h) and type of Fe oxide.

	0.64mM			**1.06mM**		
	Time h	δ^{29}Si vs.NBS28 ‰	st error $2\sigma_{\text{SEM}}$	Time h	δ^{29}Si vs.NBS28 ‰	st error $2\sigma_{\text{SEM}}$
Ferrihydrite	0	+0.02	0.07	0	+0.00	0.09
	12	+0.07	0.09	12	+0.01	0.06
	24	+0.13	0.10	48	+0.11	0.09
	48	+0.21	0.08	96	+0.22	0.09
	72 *	+0.10	0.11	288	+0.54	0.09
	192 *	+0.27	0.07	504	+0.70	0.07
Goethite	0	+0.02	0.07	0	+0.00	0.09
	12	+0.00	0.08	12	+0.02	0.07
	24	+0.13	0.08	48	+0.12	0.09
	48	+0.26	0.08	96	+0.21	0.09
	72	+0.27	0.07	288	+0.34	0.09
	192	+0.66	0.07	504	+0.50	0.08

* These values were excluded from the ${}^{29}\varepsilon$ calculation (see text and Table 10.4)

Following the Rayleigh model, ${}^{29}\varepsilon_R$ ($\pm$ $1\sigma_{SD}$) ranges between -0.57 $\pm$ 0.03‰ and -0.55 $\pm$ 0.03‰ for ferrihydrite, and between -0.85 $\pm$ 0.14‰

and -0.81 ± 0.10‰ (± $1\sigma_{SD}$) for goethite, for ic 0.64 and 1.06 mM, respectively. The fractionation factor $^{29}\varepsilon_R$ does not differ between ic solutions for a given oxide, but is significantly larger for goethite than for ferrihydrite. Following the steady state model, $^{29}\varepsilon_S$ ranges between -0.66 ± 0.06‰ and -0.99 ± 0.07‰ (± $1\sigma_{SD}$) for ferrihydrite, and between -1.17 ± 0.26‰ and -1.05 ± 0.18‰ (± $1\sigma_{SD}$) for goethite, for ic 0.64 and 1.06 m M, respectively. The fractionation factor $^{29}\varepsilon_S$ is significantly larger for goethite than for ferrihydrite at 0.64mM Si. From Table 10.4, we deduce that (i) the uncertainty on the Rayleigh $^{29}\varepsilon_R$ fractionation factor is much smaller than the one reckoned for a steady state fractionation ($^{29}\varepsilon_S$), (ii) change of ic does not affect $^{29}\varepsilon_R$ neither for ferrihydrite nor for goethite. These facts support that the progressive ^{29}Si enrichment of the solution fits a Rayleigh distillation path (Figure 10.6). Averaging our two groups of experiments at both ic solutions, our best estimates of $^{29}\varepsilon_R$ (± $1\sigma_{SD}$) are computed at -0.56 ± 0.01‰ for ferrihydrite and -0.83 ± 0.03‰ for goethite.

Table 10.4: Values of the fractionation factor $^{29}\varepsilon \pm \sigma_{SD}$ computed following Rayleigh model (R) and steady state model (S) from Eq. (10.4) and Eq. (10.5).

	Rayleigh		Steady state	
	$^{29}\varepsilon_R$	$1\sigma_{SD}$	$^{29}\varepsilon_S$	$1\sigma_{SD}$
Ferrihydrite 0.64mM *	-0.57	0.03	-0.66	0.06
Goethite 0.64mM	-0.85	0.14	-1.17	0.26
Ferrihydrite 1.06mM	-0.55	0.03	-0.99	0.07
Goethite 1.06mM	-0.81	0.10	-1.05	0.18

* excluding the δ^{29}Si measured at 72 and 192h (see text and Table 10.3)

10.4 Implications

10.4.1 Mechanisms of isotopic fractionation

Our $^{29}\varepsilon_R$ values following Rayleigh model (Table 10.4) show that the Si isotopic fractionation induced by $H_4SiO_4^0$ adsorption onto Fe oxide is similar or larger to the one generated by biological processes such as Si uptake by plants ($^{29}\varepsilon \pm 1\sigma_{SD}$ = -0.53±0.17‰, Ding et al. (2005b); -0.52±0.16‰, Ziegler et al. (2005a); -0.40±0.11‰, Opfergelt et al. (2006b); Chapter 7) and diatoms ($^{29}\varepsilon$ = -0.57±0.21‰, De La Rocha et al. (1997)).

According to Barling and Anbar (2004), the adequacy of the Rayleigh fit within our type of experimental design would indicate an irreversible

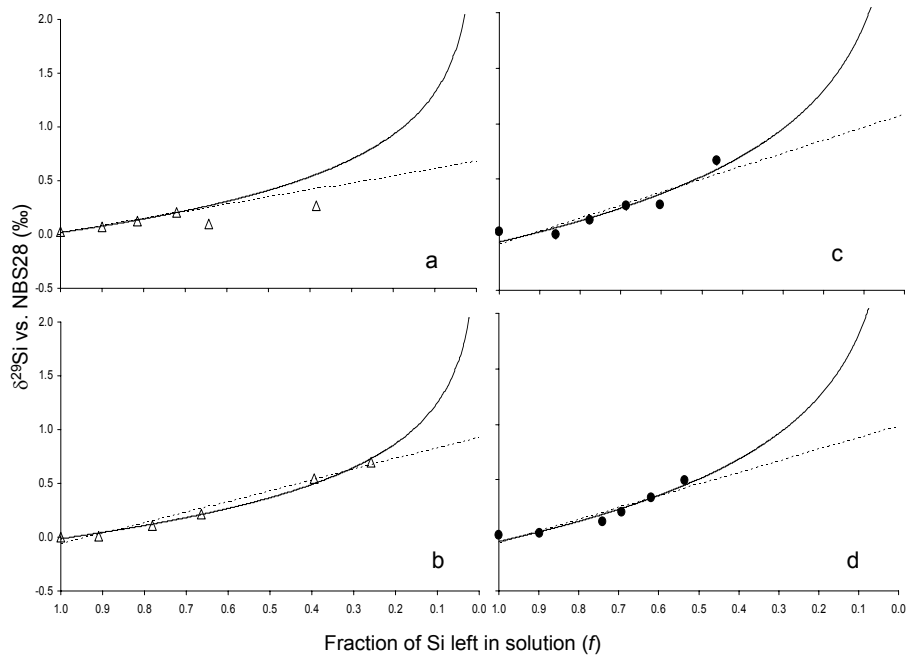

Figure 10.6: Measured Si isotopic composition (δ^{29}Si vs. NBS28) of the solution, as a function of the fraction of Si left in solution at various contact times (see Table 10.3), for ferrihydrite (a: 0.64mM Si ic - b: 1.06mM Si ic) and goethite (c: 0.64mM Si ic - d:1.06mM Si ic). The error bar ($2\sigma_{SEM}$ on single delta measurement) is included into the size of the symbol. The experimental data are compared to the best fits following Rayleigh (full lines) and steady state (dotted lines) fractionation models (see Table 10.4).

adsorption process, which would suggest a kinetic isotope effect, and thus could be associated with (i) the variation of Si adsorption rate (Figure 10.4, Table 10.3) (ii) the poor reversibility of Si adsorption through ligand exchange (Parfitt, 1978). In such a scheme, isotope fractionation can result from (i) an equilibrium fractionation between coexisting aqueous species coupled with a selective sorption of one of them (Siebert et al., 2003), (ii) the formation of inner sphere surface complexes (Lemarchand et al., 2007). In this respect, light boron isotope enrichment on goethite is strongly dependent on pH and surface complex structure (Lemarchand et al., 2007). Here, the equilibrium fractionation process between coexisting aqueous species could be discarded because $H_4SiO_4^0$ is the only significant aqueous Si species in our experimental conditions (see section 10.3.1). The Ge isotopic

fractionation during Ge sorption onto goethite privileges the selective sorption of light Ge isotopes, and has been successfully modelled by surface complexation involving the interaction of monomeric Ge hydro-complexes with $>FeOH^0$ and $>FeO^-$ sites of goethite (Galy et al., 2002b). These complexes have been further experimentally identified as Ge bi-dendate surface complexes composed of tetrahedrally coordinated Ge attached to the corners of two adjacent Fe octahedra (Pokrovsky et al., 2006). Here, we tentatively propose that the Si isotopic fractionation induced by $H_4SiO_4^0$ sorption onto ferrihydrite and goethite is caused by the formation of Fe oxide-monosilicate bi-dendate inner surface complexes ($\equiv Fe_2O_2Si(OH)_2$) (Dietzel et al., 2002; Hansen et al., 1994a; Hiemstra et al., 2007; Sigg and Stumm, 1981). However, surface Si polymerization cannot be disregarded, as the occurrence of Si tetramer has been predicted on goethite surface for Si solutions oversaturated with respect to quartz ($\sim$ 0.12 mM Si) (Hiemstra et al., 2007) (see section 10.3.1). This would hypothetically contribute to increase Si isotope fractionation for goethite relative to ferrihydrite, for which the only significant surface bonding of $H_4SiO_4^0$ should be the surface complexation of monomeric $H_4SiO_4^0$ (Hansen et al., 1994ab; Swedlund and Webster, 1999). Such an hypothesis would fit to the enrichment of light Si isotopes observed in the clay-sized fraction of soils with increasing weathering (Ziegler et al. (2005ab), Chapter 8) suggesting that clay formation may privilege light Si isotopes. Indeed, such formation in soil environment requires Si polymerization at low pressure and temperature. These hypotheses need, however, both further in-depth field-based investigations and a theoretical evaluation of the size of the isotopic energy shifts between soluble $H_4SiO_4^0$ and potential Si adsorbed polymers.

10.4.2 Environmental significance

Our data provide unequivocal answers to the four questions of critical environmental significance (see section 10.1). Si isotope fractionation (1) occurs during Si adsorption onto Fe oxide at common pH for soil solutions, (2) is similar or larger to the one generated by Si uptake by biota, and can thus contribute (3) to the depletion of light Si isotopes in river waters, and (4) to the relative concentration of light Si isotopes in soil colloidal fractions through Si sorption on pedogenic Fe oxides. Our data further suggest that the concentration of light Si isotopes in soil clay-sized fractions (Ziegler et al. (2005ab), Chapter 8) is at least partly due to $H_4SiO_4^0$ sorption onto secondary iron oxides.

Ferrihydrite and goethite are sparingly soluble constituents of weathered rocks and soils, with solubility products in the range 10^{-38} to 10^{-46} M (Schwertmann and Taylor, 1989). In well drained conditions, Fe released from weathered parent material is thus poorly mobile and accumulates in soils as secondary Fe(III) minerals: Fe oxides rapidly precipitate as discrete solid phases from the weathering solution of decomposed primary silicates. As inferred from studies on the adsorption of dissolved organic matter, juvenile oxide surfaces are very effective to adsorb solutes with which they specifically interact (Guggenberger and Kaiser, 2003). Rock weathering and soil development lead to the formation of both clay minerals and secondary oxides. These processes may thus add their mutual isotopic effects to significantly impact the Si isotopic signature of drained waters.

Si stable isotopes thus constitute a promising tracer with respect to three major processes involved in the weathering environment: biological fractionation during plant phytolith formation (Ding et al. (2005b 2008); Opfergelt et al. (2006b); Chapter 7), sequestration of Si in soil clay-sized minerals (Ziegler et al. (2005ab), Chapter 8), and adsorption of Si by pedogenic iron oxyhydroxides (this study). A similar statement concerns the Ge/Si ratio as a weathering tracer (Derry et al., 2005; Mortlock and Froelich, 1987; Scribner et al., 2006). The impact of weathering stage, soil development and free iron oxide availability on the Si isotopic composition of source and river waters thus deserves further field-based studies to progress in the appraisal of the silicon continental cycle.

10.5 Conclusion

The adsorption of $H_4SiO_4^0$ by ferrihydrite and goethite at pH 5.5 strongly fractionates Si isotopes by selectively adsorbing light isotopes and leaving a companion solution enriched with heavy Si isotopes. The isotope fractionation of silicon is similar to or larger than that generated by Si uptake by plants and diatoms. We suggest that the concentration of light Si isotopes in soil clay-sized fractions is at least partly due to $H_4SiO_4^0$ sorption onto secondary iron oxides. We conclude that rock weathering and soil development could impact the Si isotopic signature of natural waters drained to streams through Fe oxide synthesis, as oxide surfaces specifically interact with aqueous monosilicic acid.